Springer

Journal of Mechanical Science and Technology 22 (2008) 2328~2336

Journal of Mechanical Science and Technology

www.springerlink.com/content/1738-494x
DOI 10.1007/s12206-008-0909-4

The kinematic design of a planar-cam type pick-and-place device †

Wen-Tung Chang[1,*], Long-Iong Wu[2], and Chun-Hsien Liu[2]

[1]*Opto-Mechatronics Technology Center, National Taiwan University of Science and Technology, Taipei 10607, Taiwan*
[2]*Department of Power Mechanical Engineering, National Tsing Hua University, Hsinchu 30013, Taiwan*

(Manuscript Received January 16, 2008; Revised September 10, 2008; Accepted September 10, 2008)

Abstract

The planar-cam type pick-and-place device can clearly and effectively achieve the desired curvilinear motion of its end effector, and it can be designed and fabricated easily. By employing the concept of velocity instant center, the cam profiles, the paths of cutters, the pressure angles and the radii of curvature of the dual cams of the planar-cam type pick-and-place device can be expressed parametrically. The cam profiles may have concave portions, and each minimum radius of curvature of the concave portion of the dual cam profiles is the upper bound of the grinding-wheel radius that may not cause undercutting.

Keywords: Cam-modulated linkage; Curvilinear translation; Disk cam; Pick-and-place device; Profile determination

1. Introduction

Pick-and-place devices have been widely employed for the automatic material handling of assembly machines. Recently, they have also played an important role in the packaging equipment for handling chips from wafer to substrate, tray or wafer. Die bonders, chip sorters, and flip-chip bonders are some of the machines that the pick-and-place devices are frequently used for the packaging process of semiconductor and opto-electronic industry.

The end effector motion of a pick-and-place device is generally designated to perform a curvilinear translation with a path shape of inverted letter U while the orientation of the end effector remains invariant. Then, a clamping device is rigidly attached to the end effector to effectively pick and place target objects. For such a path generation, the kinematic accuracy of the start and the end positions of the end effector path is quite important. At the start position the clamping device is to pick target objects, and at the end position it is to place target objects, or vice versa.

From the viewpoint of the type synthesis of mechanisms [1, 2], the existing pick-and-place devices may be classified into the linkage type and the cam-linkage type. The parallel four-bar linkage was introduced by Lu et al. [3] to the pick-and-place machine for sorting and transporting chips from wafers to trays. In this parallel four-bar linkage, the coupler link is chosen as the end effector to trace a half-circle path, which resembles the shape of an inverted letter U. However, the higher-order kinematic characteristics of the parallel four-bar linkage are virtually constrained and cannot be designed arbitrarily; this would result in undesired accelerations and decelerations, with attendant vibration. Nagai [4] presented a cam-modulated linkage, a mechanism consisting of one or more cam-and-follower pairs in combination with a linkage [5], to perform the pick-and-place motion of the end effector, whose displacement and orientation are controlled by the groove cams. Healy [6] presented another cam-modulated linkage, the cylindrical cams combined with the linkages as the follower train,

† This paper was recommended for publication in revised form by Associate Editor Jeonghoon Yoo

*Corresponding author. Tel.: +886 2 27301123, Fax.: +886 2 27301143
E-mail address: wtchang@mail.ntust.edu.tw

to obtain the prescribed pick-and-place motion. Mink [7] recommended the roller gear cams and the linkages as the cam-modulated linkage to acquire desired motion of the end effector. MEG Corp. [8] adopted the design of planar cam-follower systems for its commercially produced pick-and-place devices.

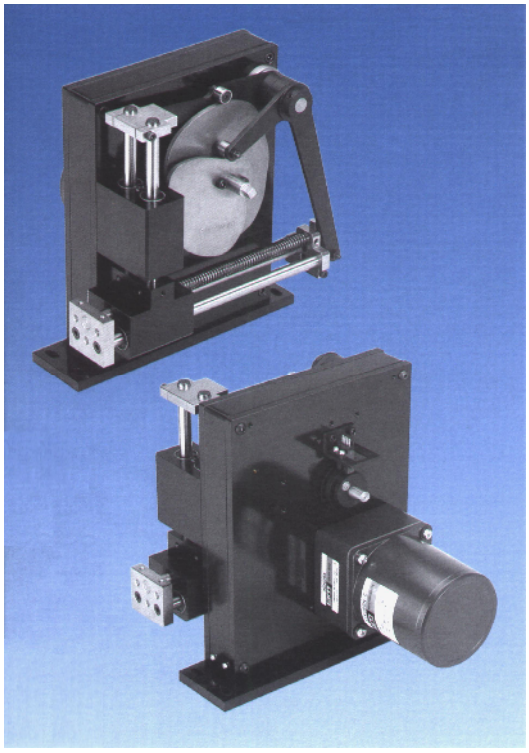

Fig. 1. The MEG X6061 pick-and-place device [8].

For these pick-and-place devices using a cam-modulated linkage, they have the common advantage that they can achieve the desired pick-and-place motion clearly and effectively. In addition, among these devices using a cam-modulated linkage, especially the ones that have planar cam-follower systems such as the MEG X6061 mechanism [8], are relatively simple to design and easy to fabricate. Nevertheless, the cam profile determination as well as the corresponding cutter path calculation for these planar cams are complicated tasks if the calculation is still based on envelope theory [9, 10] or conjugate surface theory [11-14]. Hence, this paper introduces a relatively simple analytical means for designing the pick-and-place device with planar cam-follower systems in the aspect of kinematic synthesis. Also, the MEG X6061 mechanism, a commercially available planar cam-follower type pick-and-place device, is analyzed to demonstrate the application of the method.

2. Description of the mechanism

Fig. 1 shows the MEG X6061 mechanism [8], a typical pick-and-place device of planar cam-follower

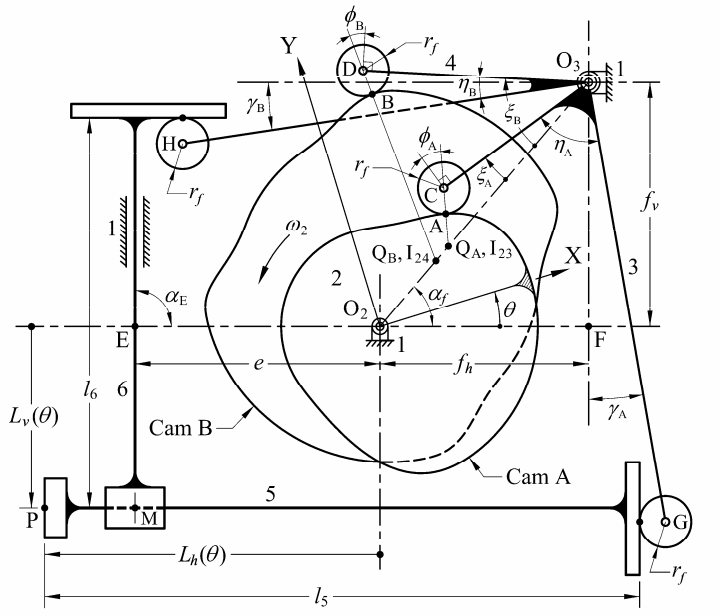

Fig. 2. Kinematic diagram of a planar cam-follower type pick-and-place device (the MEG X6061 pick-and-place device).

type, and Fig. 2 shows its kinematic diagram. In practice, return springs are used in the device to retain the intended contact of every high pair, but for clarity they are not shown in the figure. This device is in essence a cam-linkage combined mechanism. It utilizes dual cams and dual primary followers to generate the end effector motion of the follower train. The dual cams A and B are fixed on a common shaft which rotates with respect to the frame and serves as the driving link of the mechanism. For simplicity, in the following, the frame will be consistently numbered as 1, the driving link as 2, and other links are successively numbered. Cam A drives an oscillating follower (link 3), which in turn drives the end effector (link 5), a floating secondary follower, to generate the desired horizontal motion of the end effector. At the same time, cam B drives the other oscillating follower (link 4), which in turn drives a secondary translating follower (link 6) to generate the desired vertical motion of the end effector. Finally, a clamping device is rigidly attached at the left end of the end effector to effectively pick and place target objects. Because the direction of link 5 remains unchanged, the clamping device attached on the end effector produces a curvilinear translation and all points on it will trace congruent paths.

As shown in Fig. 2, dual cams A and B are both pivoted at O_2, and dual oscillating follower arms (links 3 and 4) are both pivoted at O_3. The center distance O_2O_3 can be expressed as $f = O_2O_3 = (f_h^2 + f_v^2)^{1/2}$ where f_h (= O_2F) and f_v (= O_3F) are the horizontal and vertical distance of centers, respectively. Then, the subtending angle α_f is $\tan^{-1}(f_v/f_h)$. The base circle of cam A is r_{bA} and that of cam B is r_{bB}. Rollers C and G mounted on link 3 and rollers D and H mounted on link 4 are all have the same radius of r_f. The dimensions of link 3 are $l_C = O_3C$, $l_G = O_3G$ and $\eta_A = \angle CO_3G$; the dimensions of link 4 are $l_D = O_3D$, $l_H = O_3H$ and $\eta_B = \angle DO_3H$. The distance from the right-end plate of link 5 to its reference point P is l_5; the distance from the top-end plate of link 6 to its reference point M is l_6. The center line of link 5, line PM, remains in the horizontal direction, the center line of link 6, line EM, remains in the vertical direction, and thus $\alpha_E = 90°$. The center line of link 6 has an offset of e (= O_2E) from the cam center. The cams rotate counterclockwise with a constant angular velocity of ω_2 rad/sec. Setting up a Cartesian coordinate system X-Y fixed on the driving cams and with its origin at the fixed pivot O_2, after the desired motions of the end effector with respect to the driving cams have been specified, the profile coordinates of both cams may be expressed in terms of the cam rotation angle θ, which is measured counterclockwise from the horizontal line to the X-axis.

3. The displacement functions of the end effector and the followers

As shown in Fig. 2, since all points on link 5 trace congruent paths, the desired motion of this link may be described by the path of any convenient point such as point P, the left end of this link. After the horizontal motion program $S_h(\theta)$ and the vertical motion program $S_v(\theta)$ of the reference point P have been specified, the position functions of point P relative to the cam center O_2 can consequently be expressed as the following two functions:

$$L_h(\theta) = S_h(\theta) + l_5 + r_f - f_h + l_G \cos\left\{\alpha_f + \eta_A - \cos^{-1}\left[\frac{l_C^2 + f^2 - (r_{bA} + r_f)^2}{2l_C f}\right]\right\} \quad (1)$$

and

$$L_v(\theta) = S_v(\theta) + l_6 - r_f - f_v + l_H \sin\left\{\alpha_f + \eta_B - \cos^{-1}\left[\frac{l_D^2 + f^2 - (r_{bB} + r_f)^2}{2l_D f}\right]\right\} \quad (2)$$

where $L_h(\theta)$ is the horizontal displacement function and $L_v(\theta)$ is the vertical displacement function of point P. When $\theta = 0°$, $S_h(0) = 0$ and $S_v(0) = 0$, the initial value of the horizontal displacement function will be

$$L_h(0) = l_5 + r_f - f_h + l_G \cos\left\{\alpha_f + \eta_A - \cos^{-1}\left[\frac{l_C^2 + f^2 - (r_{bA} + r_f)^2}{2l_C f}\right]\right\} \quad (3)$$

and that of the vertical displacement function will be

$$L_v(0) = l_6 - r_f - f_v + l_H \sin\left\{\alpha_f + \eta_B - \cos^{-1}\left[\frac{l_D^2 + f^2 - (r_{bB} + r_f)^2}{2l_D f}\right]\right\} \quad (4)$$

Both initial values are independent of the cam rotation angle θ. Here, functions $S_h(\theta)$ and $L_h(\theta)$ increase positively when point P moves leftward, and func-

tions $L_v(\theta)$ and $S_v(\theta)$ increase positively when point P moves downward; all of them are positive in Fig. 2. After some algebraic manipulation, the angular displacement functions of dual primary oscillating followers, O_3C and O_3D, can be respectively expressed as

$$\xi_A(\theta) = \alpha_f + \eta_A - \gamma_A(\theta) - 90^\circ$$
$$= \alpha_f + \eta_A - \cos^{-1}\left[\frac{L_h(\theta) - l_5 - r_f + f_h}{l_G}\right] \quad (5)$$

and

$$\xi_B(\theta) = \alpha_f + \eta_B - \gamma_B(\theta)$$
$$= \alpha_f + \eta_B - \sin^{-1}\left[\frac{L_v(\theta) - l_6 + r_f + f_v}{l_H}\right] \quad (6)$$

where $\gamma_A(\theta)$ ($= \alpha_f + \eta_A - \xi_A(\theta) - 90^\circ$) and $\gamma_B(\theta)$ ($= \alpha_f + \eta_B - \xi_B(\theta)$) are the angular displacement functions of oscillating arms O_3G and O_3H, respectively.

4. The cam profiles and paths of cutter centers

By employing the analytical method proposed by Wu et al. [15-19], the profile coordinates of cams A and B can be derived.

As shown in Fig. 2, by labeling velocity instant center I_{23} as Q_A and $O_2Q_A = q_A$, the speed of point Q_A on the cam A can be expressed as

$$V_{Q_A} = q_A \omega_2 \quad (7)$$

On the other hand, the speed of point Q_A on the follower O_3C (link 3) can be expressed as

$$V_{Q_A} = (f - q_A)\frac{d\xi_A(\theta)}{dt} = (f - q_A)\frac{d\xi_A(\theta)}{d\theta}\omega_2 \quad (8)$$

From Eqs. (7) and (8) and after some algebraic manipulation,

$$q_A = O_2Q_A = O_2I_{23} = f\frac{d\xi_A(\theta)}{d\theta}\Big/\left[1 + \frac{d\xi_A(\theta)}{d\theta}\right]$$
$$= \frac{fV_h(\theta)}{V_h(\theta) + \sqrt{l_G^2 - [L_h(\theta) - l_5 - r_f + f_h]^2}} \quad (9)$$

in which, $V_h(\theta) = dL_h(\theta)/d\theta = dS_h(\theta)/d\theta$ is the horizontal velocity program of point P. Likewise, by labeling velocity instant center I_{24} as Q_B and $O_2Q_B = q_B$ and after some algebraic manipulation,

$$q_B = O_2Q_B = O_2I_{24} = f\frac{d\xi_B(\theta)}{d\theta}\Big/\left[1 + \frac{d\xi_B(\theta)}{d\theta}\right]$$
$$= \frac{fV_v(\theta)}{V_v(\theta) - \sqrt{l_H^2 - [L_v(\theta) - l_6 + r_f + f_v]^2}} \quad (10)$$

in which, $V_v(\theta) = dL_v(\theta)/d\theta = dS_v(\theta)/d\theta$ is the vertical velocity program of point P. From $\triangle O_3Q_AC$ and the cosine law,

$$Q_AC = \sqrt{l_C^2 + (f - q_A)^2 - 2l_C(f - q_A)\cos\xi_A(\theta)} \quad (11)$$

From $\triangle O_3Q_BD$ and the cosine law,

$$Q_BD = \sqrt{l_D^2 + (f - q_B)^2 - 2l_D(f - q_B)\cos\xi_B(\theta)} \quad (12)$$

Then let α_A be the subtending angle between O_2O_3 and the normal line to the contact point A. From $\triangle O_3Q_AC$ and the sine law,

$$\alpha_A = \angle CQ_AO_3 = \sin^{-1}\left[\frac{l_C \sin\xi_A(\theta)}{Q_AC}\right] \quad (13)$$

Also, let α_B be the subtending angle between O_2O_3 and the normal line to the contact point B. From $\triangle O_3Q_BD$ and the sine law,

$$\alpha_B = \angle DQ_BO_3 = \sin^{-1}\left[\frac{l_D \sin\xi_B(\theta)}{Q_BD}\right] \quad (14)$$

Therefore, the vectors for the profile coordinates of cam A are

$$\mathbf{O_2A} = \mathbf{O_2Q_A} + \mathbf{Q_AA} \quad (15)$$

where

$$\mathbf{O_2Q_A} = q_A\begin{Bmatrix}\cos(\alpha_f - \theta)\\ \sin(\alpha_f - \theta)\end{Bmatrix} \quad (16)$$

and

$$\mathbf{Q_AA} = (Q_AC - r_f)\begin{Bmatrix}\cos(\alpha_f + \alpha_A - \theta)\\ \sin(\alpha_f + \alpha_A - \theta)\end{Bmatrix} \quad (17)$$

Similarly, the vectors for the profile coordinates of cam B are

$$\mathbf{O_2B} = \mathbf{O_2Q_B} + \mathbf{Q_BB} \quad (18)$$

where

$$\mathbf{O_2Q_B} = q_B\begin{Bmatrix}\cos(\alpha_f - \theta)\\ \sin(\alpha_f - \theta)\end{Bmatrix} \quad (19)$$

and

$$\mathbf{Q_BB} = (Q_BD - r_f)\begin{Bmatrix}\cos(\alpha_f + \alpha_B - \theta)\\ \sin(\alpha_f + \alpha_B - \theta)\end{Bmatrix} \quad (20)$$

Hence, the parametric vector equations of the respective profile coordinates of cams A and B are

$$\mathbf{O}_2\mathbf{A}=\begin{Bmatrix}x_{\mathrm{A}}(\theta)\\ y_{\mathrm{A}}(\theta)\end{Bmatrix}$$
$$=\begin{Bmatrix}q_{\mathrm{A}}\cos(\alpha_f-\theta)+(\mathrm{Q_AC}-r_f)\cos(\alpha_f+\alpha_{\mathrm{A}}-\theta)\\ q_{\mathrm{A}}\sin(\alpha_f-\theta)+(\mathrm{Q_AC}-r_f)\sin(\alpha_f+\alpha_{\mathrm{A}}-\theta)\end{Bmatrix} \quad (21)$$

and

$$\mathbf{O}_2\mathbf{B}=\begin{Bmatrix}x_{\mathrm{B}}(\theta)\\ y_{\mathrm{B}}(\theta)\end{Bmatrix}$$
$$=\begin{Bmatrix}q_{\mathrm{B}}\cos(\alpha_f-\theta)+(\mathrm{Q_BD}-r_f)\cos(\alpha_f+\alpha_{\mathrm{B}}-\theta)\\ q_{\mathrm{B}}\sin(\alpha_f-\theta)+(\mathrm{Q_BD}-r_f)\sin(\alpha_f+\alpha_{\mathrm{B}}-\theta)\end{Bmatrix} \quad (22)$$

From $\triangle \mathrm{O_3Q_AC}$, the pressure angle ϕ_{A} can be expressed as [15, 16, 19, 20]

$$\phi_{\mathrm{A}}=90^\circ-\alpha_{\mathrm{A}}-\xi_{\mathrm{A}}(\theta) \quad (23)$$

From $\triangle \mathrm{O_3Q_BD}$, the pressure angle ϕ_{B} can be expressed as [15, 16, 19, 20]

$$\phi_{\mathrm{B}}=90^\circ-\alpha_{\mathrm{B}}-\xi_{\mathrm{B}}(\theta) \quad (24)$$

In practice, the cutter or grinding wheel is frequently chosen larger than the follower roller for reasonable grinding wear life and better cam surface irregularities [21]. The instantaneous locations of the cutters for cutting the profiles of cams A and B are shown in Fig. 3. Because the cutter and roller centers must lie on a common normal to the cam profile [15, 18, 21], normally outward extending the cam profile by a length of cutter radius r_c obtains the location of the cutter center. In other words, for cam A, the cutter center $\mathrm{T_A}$ and point $\mathrm{Q_A}$ ($\mathrm{I_{23}}$) as well as points A and C must always lie on a line. Also, for cam B, the cutter center $\mathrm{T_B}$ and point $\mathrm{Q_B}$ ($\mathrm{I_{24}}$) as well as points B and D must always lie on a line. Therefore, the parametric equations for the coordinates of the cutter center $\mathrm{T_A}$ are

$$\mathbf{O}_2\mathbf{T}_{\mathrm{A}}=\mathbf{O}_2\mathbf{Q}_{\mathrm{A}}+\mathbf{Q}_{\mathrm{A}}\mathbf{T}_{\mathrm{A}} \quad (25)$$

where

$$\mathbf{Q}_{\mathrm{A}}\mathbf{T}_{\mathrm{A}}=(\mathrm{Q_AC}-r_f+r_c)\begin{Bmatrix}\cos(\alpha_f+\alpha_{\mathrm{A}}-\theta)\\ \sin(\alpha_f+\alpha_{\mathrm{A}}-\theta)\end{Bmatrix} \quad (26)$$

The location of the cutter center $\mathrm{T_B}$ for cutting cam B can also be located in the same way:

$$\mathbf{O}_2\mathbf{T}_{\mathrm{B}}=\mathbf{O}_2\mathbf{Q}_{\mathrm{B}}+\mathbf{Q}_{\mathrm{B}}\mathbf{T}_{\mathrm{B}} \quad (27)$$

where

$$\mathbf{Q}_{\mathrm{B}}\mathbf{T}_{\mathrm{B}}=(\mathrm{Q_BD}-r_f+r_c)\begin{Bmatrix}\cos(\alpha_f+\alpha_{\mathrm{B}}-\theta)\\ \sin(\alpha_f+\alpha_{\mathrm{B}}-\theta)\end{Bmatrix} \quad (28)$$

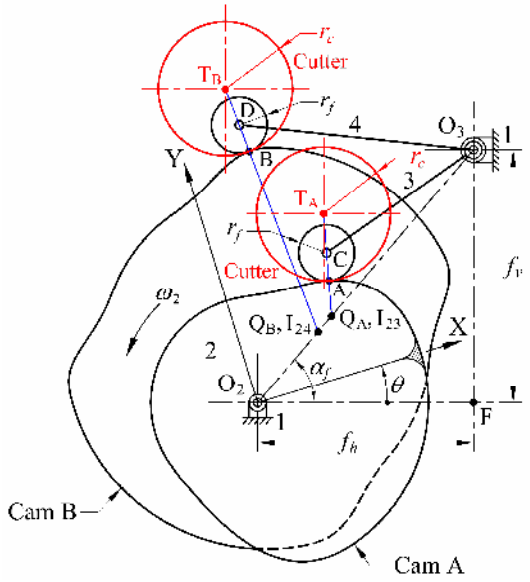

Fig. 3. Locations of the cutter centers for cutting the cam profiles.

Hence, the parametric vector equations of the cutter center coordinates are

$$\mathbf{O}_2\mathbf{T}_{\mathrm{A}}=\begin{Bmatrix}x_{\mathrm{T_A}}(\theta)\\ y_{\mathrm{T_A}}(\theta)\end{Bmatrix}$$
$$=\begin{Bmatrix}q_{\mathrm{A}}\cos(\alpha_f-\theta)+(\mathrm{Q_AC}-r_f+r_c)\cos(\alpha_f+\alpha_{\mathrm{A}}-\theta)\\ q_{\mathrm{A}}\sin(\alpha_f-\theta)+(\mathrm{Q_AC}-r_f+r_c)\sin(\alpha_f+\alpha_{\mathrm{A}}-\theta)\end{Bmatrix} \quad (29)$$

and

$$\mathbf{O}_2\mathbf{T}_{\mathrm{B}}=\begin{Bmatrix}x_{\mathrm{T_B}}(\theta)\\ y_{\mathrm{T_B}}(\theta)\end{Bmatrix}$$
$$=\begin{Bmatrix}q_{\mathrm{B}}\cos(\alpha_f-\theta)+(\mathrm{Q_BD}-r_f+r_c)\cos(\alpha_f+\alpha_{\mathrm{B}}-\theta)\\ q_{\mathrm{B}}\sin(\alpha_f-\theta)+(\mathrm{Q_BD}-r_f+r_c)\sin(\alpha_f+\alpha_{\mathrm{B}}-\theta)\end{Bmatrix} \quad (30)$$

5. The radii of curvatures

Due to practical design considerations such as contact stress, grinding-wheel radius, and undercutting, it might be necessary to determine the radii of curvatures of the cam profiles. Since the parametric vector equations of the cam profiles have been derived, their corresponding radii of curvatures can also be determined, either analytically or numerically. From Eqs. (21) and (22), the radii of curvatures of cams A and B,

ρ_A and ρ_B, can be respectively expressed as [22]

$$\rho_A(\theta) = \frac{(x'^2_A + y'^2_A)^{1.5}}{x'_A y''_A - x''_A y'_A} \tag{31}$$

and

$$\rho_B(\theta) = \frac{(x'^2_B + y'^2_B)^{1.5}}{x'_B y''_B - x''_B y'_B} \tag{32}$$

where the prime denotes differentiation with respect to the cam rotation angle θ. The analytical expressions of the differential terms appearing in Eqs. (31) and (32) are extremely complicated to be practicable and thus are not shown here; to solve them numerically is suggested instead.

The radius of curvature may be either positive or negative depending on the convexity of the cam profile. In Fig. 2, it is positive for the concave portion of the cam because of the sense on the cam profile corresponding to increasing θ [22]. In the following context, the radii of curvatures are labeled as ρ_A^+ and ρ_B^+ if they are positive (which represents the concave portion of the cam), and they are labeled as ρ_A^- and ρ_B^- if they are negative (which represents the convex portion of the cam). To avoid the undercutting situation in the cam cutting process, the cutter or grinding-wheel radius must be always smaller than the minimum radius of curvature of the concave portion of the cam. That is, for cam A, the cutter or grinding-wheel radius is limited by

$$r_c < (\rho_A^+)_{\min} \tag{33}$$

For cam B, the cutter or grinding-wheel radius is limited by

$$r_c < (\rho_B^+)_{\min} \tag{34}$$

6. Example

The kinematic design of the pick-and-place device will be illustrated by the following example.

In this case, the specified motion programs, $S_h(\theta)$ and $S_v(\theta)$, are shown in Fig. 4(a). Such motion programs can lead to the resulting path of point P as shown in Fig. 4(b). That is, point P will successively occupy positions P_0, P_1, P_2, P_3, ... with P_0 being the initial position. In addition, the path positions of point P are correlated with cam rotation angles. Point P stays at its initial position P_0 while the cams rotate counterclockwise from 0° to 13°, then moves downward via P_1 to its first working position P_2 for 40° cam rotation, and then dwells for the next 30°. When the cams rotate from 83° to 123°, point P moves upward from position P_2 via P_3 to position P_4; during this period, when θ = 106°, point P also starts its leftward motion at position P_3, simultaneously. When the cams rotate from 123° to 178°, point P moves leftward from position P_4 to position P_5. From θ = 178° to θ = 218°, point P moves downward again from position P_5 via P_6 to position P_7, its second working position, and then dwells for the next 30°; during this period, when θ = 195°, point P completes its leftward motion at P_6. From θ = 248° to θ = 288°, tracing the former path, point P moves upward from position P_7 via P_8 to position P_9. Then from position P_9, it moves rightward to position P_0 for the next 72°. During this period, when θ = 271°, it must occupy position P_8. The horizontal and vertical travel lengths of point P are 100 and 30 mm, respectively, both with cycloidal motions.

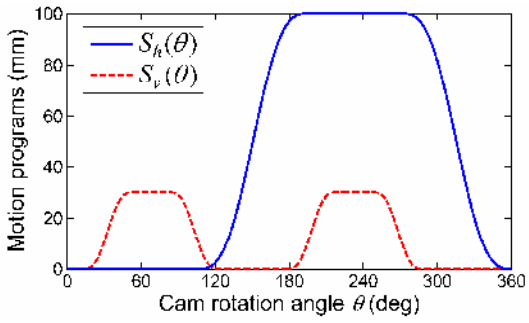

(a)

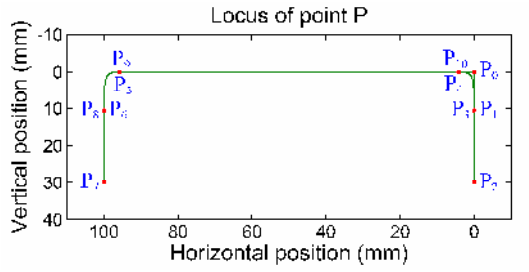

(b)

Fig. 4. Motion programs and locus of the functional output (the reference point P) of a pick-and-place device.

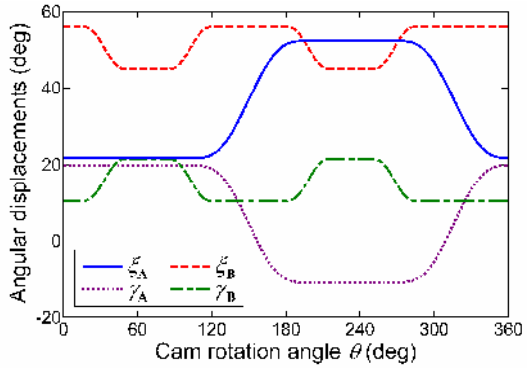

Fig. 5. Angular displacements of the oscillating followers in a pick-and-place device.

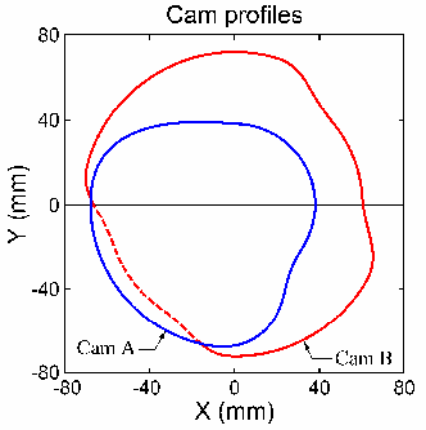

Fig. 6. Profiles of cams A and B in a pick-and-place device.

Other dimensions of the design parameters are: f_h = 60 mm, f_v = 75 mm, $l_C = l_D$ = 60 mm, l_G = 190 mm, l_H = 160 mm, η_A = 80°, η_B = 15°, r_f = 8 mm, r_{bA} = 38 mm, r_{bB} = 72 mm, l_5 = 230 mm, l_6 = 200 mm, e = 100 mm and α_E = 90°. The magnitude of offset e will not affect cam profiles. Figure 5 shows the angular displacements of the oscillating followers. The determined cam profiles and their corresponding pressure angles ϕ_A and ϕ_B together with radii of curvatures ρ_A and ρ_B are shown in Figs. 6, 7 and 8, respectively. The cams A and B have their maximum radial dimensions of 68.008 and 72 mm, respectively, while the extremes of the pressure angles and the radii of curvatures are all listed in Table 1. Both cam profiles have concave and convex portions. Two inflection points occur at the contour of cam A, while eight inflection points occur at that of cam B; at these inflection

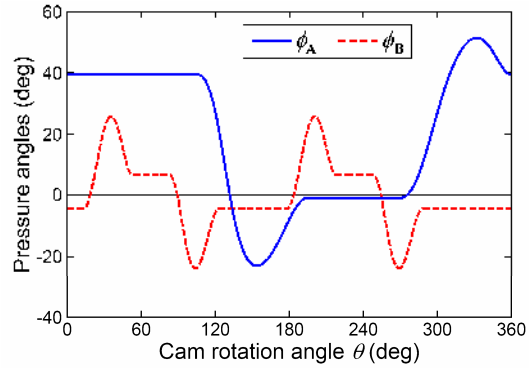

Fig. 7. Pressure angles of cams A and B in a pick-and-place device.

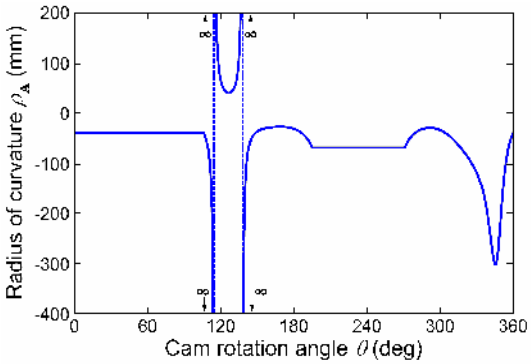

(a)

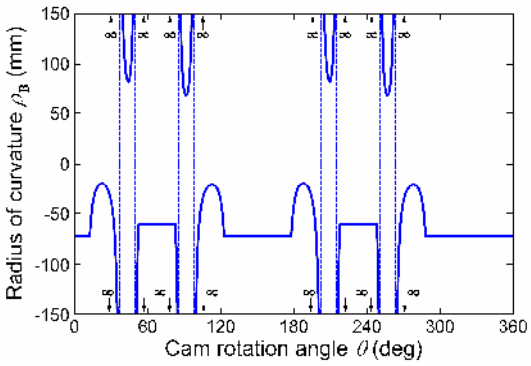

(b)

Fig. 8. Radii of curvatures of cams A and B in a pick-and-place device.

points, the cam contours lead to zero curvatures (infinite radii of curvatures). At θ = 126.84°, the concave portion of the profile of cam A has its minimum radius of curvature of 42.22 mm, which is the upper bound of the cutter or grinding-wheel radius that may

Table 1. Input angles and extreme values.

Input angle	Extreme value
$\theta = 22.88°$	$(\rho_B^-)_{max} = -19.73$ mm
$\theta = 35.63°$	$(\phi_B)_{max} = 25.81°$
$\theta = 91.86°$	$(\rho_B^+)_{min} = 67.96$ mm
$\theta = 103.92°$	$(\phi_B)_{min} = -23.77°$
$\theta = 126.84°$	$(\rho_A^+)_{min} = 42.22$ mm
$\theta = 153.75°$	$(\phi_A)_{min} = -23.02°$
$\theta = 168.81°$	$(\rho_A^-)_{max} = -26.71$ mm
$\theta = 187.88°$	$(\rho_B^-)_{max} = -19.73$ mm
$\theta = 200.63°$	$(\phi_B)_{max} = 25.81°$
$\theta = 256.86°$	$(\rho_B^+)_{min} = 67.96$ mm
$\theta = 268.92°$	$(\phi_B)_{min} = -23.77°$
$\theta = 331.91°$	$(\phi_A)_{max} = 51.5°$

not cause undercutting. Also, the maximum allowable cutter or grinding-wheel radius for machining the profile of cam B is 67.96 mm, which is the minimum radius of curvature of concave portions of this cam profile occurring at $\theta = 91.86°$ and $\theta = 256.86°$. The maximum pressure angle of cam A occurs at $\theta = 331.91°$ and has a magnitude of 51.5°, which is larger than 45°, the recommended upper bound of the pressure angle for disk cam mechanisms with an oscillating roller follower [23]. However, this situation could be endurable if the carrying load of the pick-and-place device is small enough.

7. Conclusions

The pick-and-place device plays an important role in the packaging equipment for handling chips from wafer to substrate, tray or wafer. The end effector motion of a pick-and-place device is generally designated to perform a curvilinear translation with a path shape of inverted letter U while the orientation of the end effector remains invariant. The pick-and-place device of the cam-modulated linkage type with planar cam-follower systems, such as the MEG X6061 mechanism, can be designed and fabricated easily and also has the advantage of being able to achieve the desired pick-and-place motion clearly and effectively. By employing the concept of velocity instant center, the cam profiles, the paths of cutters, the pressure angles and the radii of curvature of the dual cams of the MEG X6061 mechanism can be expressed parametrically. The profiles of the dual cams may have concave and convex portions, and each minimum radius of curvature of the concave portion of the dual cam profiles is the upper bound of the grinding-wheel radius that may not cause undercutting.

Acknowledgment

The authors are grateful to the National Science Council of the Republic of China for supporting this research under Grant No. NSC-92-2212-E-007-056.

References

[1] R. S. Hartenberg and J. Denavit, *Kinematic Synthesis of Linkages*, McGraw-Hill, New York, USA, (1964), 130-147.

[2] G. N. Sandor and A. G. Erdman, *Advanced Mechanism Design: Analysis and Synthesis, Volume 2*, Prentice-Hall, Englewood Cliffs, New Jersey, USA, (1984), 49-176.

[3] W. J. Lu, C. Y. Liu, Y. T. Wan, C. K. Lai, C. H. Huang, C. M. Lin, and C. H. Liu, Device for Fast Taking out and Putting in, US Patent 6505528, (2003).

[4] S. Nagai, Gate Motion Mechanism, US Patent 3988938, (1976).

[5] A. G. Erdman, G. N. Sandor, and S. Kota, *Mechanism Design: Analysis and Synthesis, Volume 1*, Fourth Ed., Prentice-Hall, Englewood Cliffs, New Jersey, USA, (2001), 426-435.

[6] F. L. Healy, Parts Handler, US Patent 3865253, (1975).

[7] G. Mink, Article Handling Device, Great Britain Patent 2046201, (1980).

[8] Machine Engineering (MEG) Corp., *Products Guide Book (in Japanese)*, MEG Corp., Nagano, Japan, (1996), 74-81.

[9] R. S. Hanson and F. T. Churchill, Theory of envelopes provides new cam design equations, *Product Engineering*, August 20 (1962) 45-55.

[10] C. E Wilson and J. P. Sadler, *Kinematics and Dynamics of Machinery*, Third Ed. (International Ed.), Prentice-Hall, Upper Saddle River, New Jersey, USA, (2003), 364-388.

[11] J. Chakraborty and S. G. Dhande, *Kinematics and Geometry of Planar and Spatial Cam Mechanisms*, Wiley Eastern, New Delhi, India, (1977), 1-66.

[12] J. L. Meng, K. E. Hsieh, and C. B. Tsay, An analytical method for synthesis of cam profiles, *Journal of the Chinese Society of Mechanical Engineers*, 8 (4) (1987) 271-276.
[13] F. L. Litvin, *Theory of Gearing*, NASA Reference Publication 1212, Washington D.C., USA, (1989), 63-86, 166-214.
[14] F. L. Litvin, *Gear Geometry and Applied Theory*, Prentice-Hall, Englewood Cliffs, New Jersey, USA, (1994), 107-159.
[15] L. I. Wu, Calculating conjugate cam profiles by vector equations, *Proceedings of the Institution of Mechanical Engineers—Part C, Journal of Mechanical Engineering Science*, 217 (10) (2003) 1117-1123.
[16] L. I. Wu and W. T. Chang, Analysis of mechanical errors in disc cam mechanisms, *Proceedings of the Institution of Mechanical Engineers—Part C, Journal of Mechanical Engineering Science*, 219 (2) (2005) 209-224.
[17] W. T. Chang and L. I. Wu, Mechanical error analysis of disk cam mechanisms with a flat-faced follower, *Journal of Mechanical Science and Technology*, 20 (3) (2006) 345-357.
[18] L. I. Wu, W. T. Chang, and C. H. Liu, The design of varying-velocity translating cam mechanisms, *Mechanism and Machine Theory*, 42 (3) (2007) 352-364.
[19] W. T. Chang, L. I. Wu, K. H. Fuh, and C. C. Lin, Inspecting profile errors of conjugate disk cams with coordinate measurement, *Transactions of the ASME, Journal of Manufacturing Science and Engineering*, 130 (1) (2008) 011009.
[20] W. T. Chang and L. I. Wu, A simplified method for examining profile deviations of conjugate disk cams, *Transactions of the ASME, Journal of Mechanical Design*, 130 (5) (2008) 052601.
[21] H. A. Rothbart, *Cams: Design, Dynamics, and Accuracy*, John Wiley, New York, USA, (1956), 78-89.
[22] R. Courant and F. John, *Introduction to Calculus and Analysis, Volume 1*, Interscience, New York, USA, (1965), 354-360.
[23] P. W. Jenson, *Cam Design and Manufacture*, Second Ed., Marcel Dekker, New York, USA, (1987), 76.

Wen-Tung Chang received his Bachelor and Master degrees in Mechanical and Marine Engineering from Nation Taiwan Ocean University in 2000 and 2002, respectively. He then went on to receive his Ph.D. degree in Power Mechanical Engineering from National Tsing Hua University in 2007. Dr. Chang is currently a Postdoctoral Researcher of Opto-Mechatronics Technology Center at National Taiwan University of Science and Technology in Taipei, Taiwan. His research interests include kinematics and dynamics of machinery, mechanism and machine design, and opto-mechatronic system.

Long-Iong Wu received his Ph.D. degree in Mechanical Engineering from National Cheng Kung University in 1987. Dr. Wu is currently a Professor of Department of Power Mechanical Engineering at National Tsing Hua University in Hsinchu, Taiwan. His research interests include kinematics of machinery, mechanism design, and precision machine design. His main research activities in his laboratory are linkage mechanism design and cam mechanism design. In the past, Dr. Wu has worked for China Steel Corp., and San Shing Fastech Corp. where he was responsible for designing high speed nut formers.

Chun-Hsien Liu received his Master degree in Mechanical Engineering from Nation Chiao Tung University in 1996. He is currently a Lecturer and also a Ph.D. Candidate of Department of Power Mechanical Engineering at National Tsing Hua University in Hsinchu, Taiwan. Mr. Liu has worked for over twenty years at Industrial Technology Research Institute (ITRI), where he was responsible for designing packaging equipments in semiconductor and flat panel display industry. He is currently the Deputy Director of Intelligent Systems Engineering Division of Mechanical and Systems Research Laboratories at ITRI.